Bioorganic & Medicinal Chemistry Letters 22 (2012) 2497–2502

Contents lists available at SciVerse ScienceDirect

Bioorganic & Medicinal Chemistry Letters

journal homepage: www.elsevier.com/locate/bmcl

Thiadiazoles as new inhibitors of diacylglycerol acyltransferase type 1

Patrick Mougenot [a,*], Claudie Namane [a], Eykmar Fett [a], Florence Camy [a], Rommel Dadji-Faïhun [a], Gwladys Langot [a], Catherine Monseau [a], Bénédicte Onofri [a], François Pacquet [a], Cécile Pascal [a], Olivier Crespin [a], Majdi Ben-Hassine [a], Jean-Luc Ragot [a], Thao Van-Pham [a], Christophe Philippo [a], Florence Chatelain-Egger [a], Philippe Péron [a], Jean-Christophe Le Bail [a], Etienne Guillot [a], Philippe Chamiot-Clerc [a], Marie-Aude Chabanaud [a], Marie-Pierre Pruniaux [a], Friedemann Schmidt [b], Olivier Venier [a], Eric Nicolaï [a,*], Fabrice Viviani [a]

[a] Sanofi-aventis R&D, Early to Candidate Unit, 1 avenue Pierre Brossolette, 91385 Chilly-Mazarin, France
[b] Sanofi-aventis Deutschland GmbH, Lead Generation to Candidate Realization, Design & Informatics, Industriepark Hoechst, 65926 Frankfurt am Main, Germany

ARTICLE INFO

Article history:
Received 16 December 2011
Revised 31 January 2012
Accepted 2 February 2012
Available online 15 February 2012

Keywords:
Diacylglycerol acyltransferase type 1
DGAT-1 inhibitors
Triacylglycerides inhibition
Thiadiazole
Pharmacodynamic in vivo assay

ABSTRACT

A novel class of DGAT1 inhibitors containing a thiadiazole core has been discovered. Chemical optimization lead to inhibitors of human DGAT1 with an appropriate ADME profile and that show in vivo activity in target tissues.

Triacylglycerides (TG) are the principal form of energy storage in eukaryotes. An imbalance in the metabolism of triacylglycerides can participate in the pathogenesis of several metabolic disorders such as obesity, insulin resistance and type 2 diabetes.[1]

DGAT-1, diacylglycerol acyltransferase type 1 catalyses the last step of triacylglyceride biosynthesis, transforming diacylglycerol and acyl-CoA into triacylglycerides. Two isoforms of diacylglycerol acyltransferase have been described: DGAT-1[2] and DGAT-2.[3] DGAT-1 and DGAT-2 show 12% homology in their amino acid sequences. In mammals, DGAT-1 is widely expressed, particularly in the intestine, skeletal muscle, and testis while DGAT-2 is widely expressed with high expression levels in the liver and adipose tissues.

Potential beneficial therapeutic effects of DGAT-1 inhibition are supported by DGAT-1 silencing studies. Indeed, DGAT-1 deficient mice are resistant to diet-induced obesity, have lower plasma glucose levels associated with an increase of insulin and leptin sensitivity and are also protected against diet-induced hepatic steatosis.[4] In addition, DGAT-1 anti-sense oligonucleotide injection reduces the fibrosis promoted by a methionine/choline deficient diet.[5] Moreover, small molecule DGAT-1 inhibitors improve physiological parameters such as TG or glucose homeostasis in rodent preclinical models of metabolic disorders.[6]

Bayer and Japan Tobacco first reported potent DGAT-1 inhibitors in 2004.[7] Despite a strong interest and the efforts of the pharmaceutical industry, very few compounds have reached and are currently undergoing clinical trials since that time, for example, LCQ-908 (structure not disclosed) from Novartis in phase II, AZD-7687 (structure not disclosed) from Astra-Zeneca and PF-04620110 from Pfizer reported in phase I (Fig. 1).[8]

We aimed to identify new DGAT-1 inhibitors by combining ligand-based modeling from known DGAT-1 inhibitors,[9] high throughput parallel synthesis (HTPS) and rescaffolding chemistry to generate leads amenable to optimization. Three lead series were thus found with IC_{50}s below 100 nM in a DGAT-1 enzymatic assay.[10]

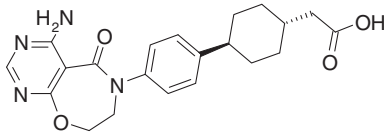

Figure 1. PF-04620110 in phase I.

* Corresponding authors.
E-mail address: patrick.mougenot@sanofi-aventis.com (P. Mougenot).

0960-894X/$ - see front matter © 2012 Elsevier Ltd. All rights reserved.
doi:10.1016/j.bmcl.2012.02.006

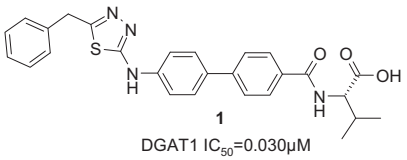

Figure 2. Lead compound **1** from aminothiadiazole series.

The most potent inhibitors belonged to a 2-aminothiadiazole series represented by compound **1** which displayed an IC_{50} of 0.03 μM in the enzymatic assay (Fig. 2).

The synthesis of the aminothiadiazole **1** started from aniline **2**[11] which reacted with thiocarbonyldiimazole and phenylacetic hydrazide to afford intermediate **3**. Cyclization of **3** produced the aminothiadiazole **4**. In the last step, ester hydrolysis gave the acid compound **1** (Scheme 1).

Compound **1** showed encouraging functional cellular activity, with an IC_{50} of 0.30 μM in an assay measuring the ability of inhibitors to decrease TG synthesis in Chang liver cells[12] but suffered from a low value in the Caco-2 permeability model (0.4×10^{-7}-cm s^{-1}). We suspected that the permeability issue was mainly due to a too high polarity (TPSA = 132)[13] of the molecule and in particular the presence of the benzoylvaline moiety, but attempts at its modulation failed to give better permeability properties (data not shown). Since the presence of a carboxylic acid turned out to be critical, we looked for potential benzoylvaline surrogates which would retain good inhibitory activity and improve permeability, including the grafting of the phenylcyclohexane acetic acid fragment to the 2-aminothiadiazole scaffold, thus leading to compound **9**.

The synthesis of compound **9** started from the commercially available intermediate **5**. The phenol **5** gave the alkene **6** after a Horner–Emmons reaction. The subsequent hydrogenation followed by a triflation reaction led to the intermediate **8**. Finally, the Buchwald reaction afforded the expected compound **9** as a mixture of cis/trans (35:65) stereoisomers (Scheme 2).

Surprisingly, compound **9** was completely inactive, with an IC_{50} above 10 μM in the DGAT-1 enzymatic assay.

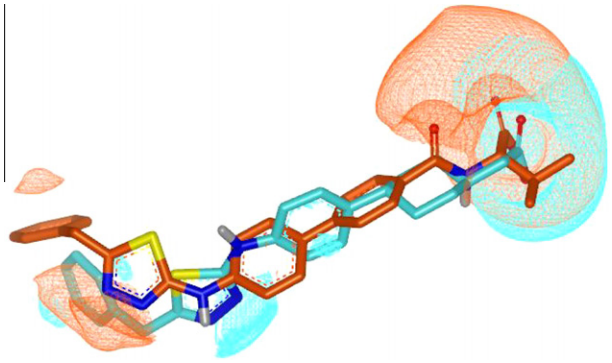

Figure 3. Ligand-based alignment for compound **1** (shown in red) and compound **9a** (shown in light blue), electrostatic negative isovalue maps[9] (at level −0.9 for each compound). Poor overlap of the thiadiazole scaffolds is observed. The interatomic distance between the aniline hydrogen N(H) and the carboxylate (C)OOH varies from 13.07 Å in compound **1** to 11.37 Å in compound **9a**.

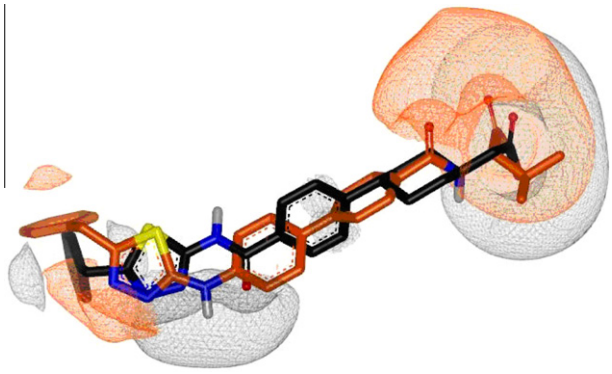

Figure 4. Ligand-based alignment for compound **1** (shown in red) and compound **10** (shown in black), electrostatic negative isovalue maps[9] (at level −0.9 for each compound). In contrast to compound **9a**, the thiadiazole scaffolds of compound **1** and **10** overlap significantly, forming a shared negative patch alongside the thiadiazole nitrogens which indicates a recognition feature. The interatomic distance between the aniline hydrogen N(H) and the carboxylate (C)OOH of compound **10** is 11.38 Å.

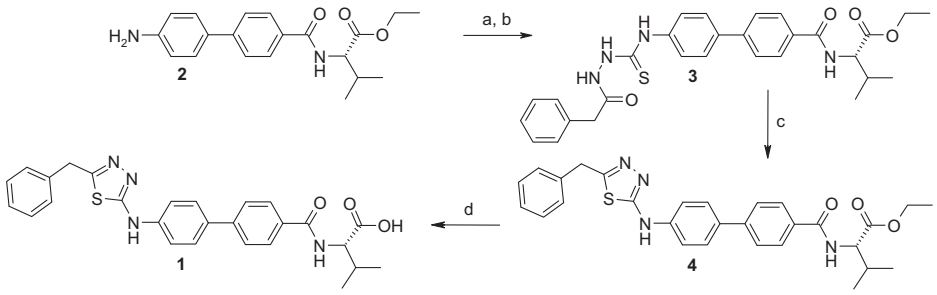

Scheme 1. Synthesis of compound **1**. Reagents and conditions: (a) 1,1′-thiocarbonyldiimidazole, DMF, rt; (b) phenylacetic hydrazide, EtOH, reflux, overnight, 49%, two steps; (c) H_2SO_4, 0 °C, 1 h; (d) LiOH, THF, MeOH, H_2O, rt, 83% (two steps).

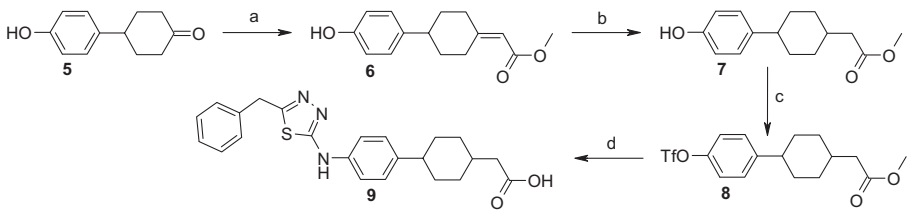

Scheme 2. Synthesis of compound **9**. Reagents and conditions: (a) methyl diethylphosphonoacetate, NaH, THF, rt; (b) H_2, Pd/C (10%), THF; (c) Tf_2O, DIEA, CH_2Cl_2, 0 °C, overnight, 49%, three steps; (d) 5-benzyl-1,3,4-thiadiazol-2-amine, Pd_2dba_3, S-Phos, NaOtBu, toluene, reflux, 7%.

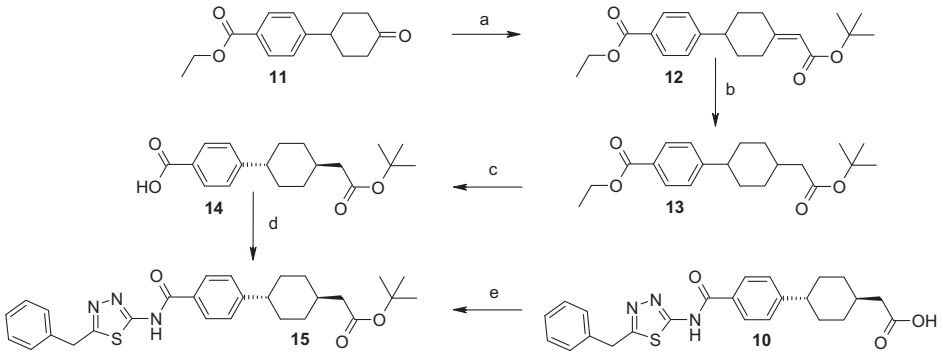

Scheme 3. Synthesis of compound **10**. Reagents and conditions: (a) *tert*-butyl diethylphosphonoacetate, NaH, THF, RT, 18 h, 72%; (b) H_2 (35 psi), Pd/C (10%), EtOH, 3 h, 86%; (c) LiOH, THF, MeOH, H_2O, rt, overnight, 50% after recrystallization from ethyl acetate; (d) 5-benzyl-1,3,4-thiadiazol-2-amine, EDC, HOBt, DIPEA, DMF, CH_2Cl_2, rt, 4 days, 68%; (e) TFA, CH_2Cl_2, 92%.

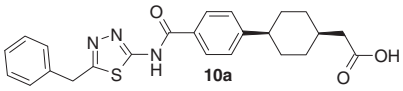

Figure 5. Compound **10a**.

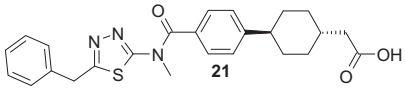

enz. DGAT1 IC_{50}>10μM
cell. DGAT-1 ND

Figure 6. Compound **21**.

To understand this loss of activity, we used a ligand-based 3D alignment model[9] to compare compounds **1** and **9a** (trans isomer). In Figure 3, the alignment of compounds **1** and **9a** shows that, although there is good shape similarity, the thiadiazole in **9a** is geometrically distorted compared to **1**.

This observation prompted us to modify the linker between the thiadiazole and the phenylcyclohexyl group. Of all the chemical modifications proposed and filtered using ligand-based alignment, we selected the amide group as the preferred linker. This choice was supported by the ligand-based alignment for compounds **1** and **10** (with CO inserted) which showed that the amide linker retains a high shape similarity and provides excellent matching of the thiadiazoles (Fig. 4).

The synthesis of compound **10** is depicted in Scheme 3, starting with the preparation of the ketone **11** as previously described.[15] Subsequent Horner–Emmons reaction afforded the alkene **12**. Hydrogenation followed by hydrolysis and then recrystallization gave intermediate **14** with the trans configuration. Finally, the coupling reaction with commercially available 5-benzyl-1,3,4-thiadiazol-2-amine followed by the cleavage of the *tert*-butyl ester led to the expected carboxylic acid **10**.

The use of the amide linker restored DGAT-1 inhibition with compound **10** displaying good enzymatic activity (IC_{50} = 0.036 μM). Moreover, contrary to compound **1**, this derivative also displayed a similar level of activity in the cellular assay (IC_{50} = 0.029 μM). There was also an improvement of Caco-2 permeability (112×10^{-7}-cm s^{-1}). Compound **10** was also found stable in metabolic stability studies (< or equal to 5% transformation in human or mouse hepatic microsomes).

Starting from compound **10**, we first explored the effects of modifying the acidic moiety. In the same manner as described in Scheme 3, but using a cis/trans mixture of intermediate **14**, and HPLC separation of the final compound[14], we obtained the cis isomer of compound **10** (Fig. 5).

This cis cyclohexyl stereoisomer **10a** was found to be 15 times less potent (IC_{50} = 0.578 μM) than the trans isomer **10** in the enzymatic assay.

Replacing the cyclohexylacetic acid moiety by cyclohexylpropionic acid gave rise to compound **10b** and a 10-fold drop in activity (IC_{50} = 0.35 μM).

The synthesis of compound **10b** is depicted in Scheme 4 starting from the ketone **11**. Subsequent reaction with trimethylsulfoxonium iodide gave epoxide **16**. Treatment with boron trifluoride etherate afforded the aldehyde **17** which was then engaged in a Horner–Emmons reaction to yield the trans alkene **18** after chromatography. Hydrogenation followed by a basic hydrolysis gave

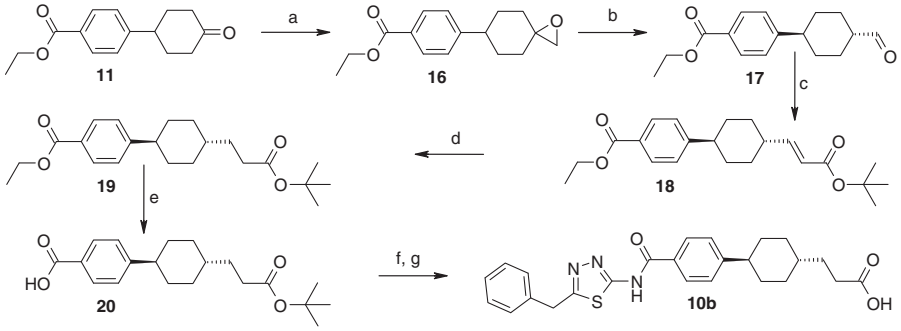

Scheme 4. Synthesis of compound **10b**. Reagents and conditions: (a) trimethylsulfoxonium iodide, NaH, THF, DMSO, 50 °C, 1 h, 46%; (b) $BF_3{\cdot}Et_2O$, CH_2Cl_2, rt, 3 h, 81%; (c) *tert*-butyl diethylphosphonoacetate, NaH, THF, rt, 18 h; (d) H_2, Pd/C (10%), EtOH, 3 h, 79%, two steps; (e) LiOH, THF, MeOH, H_2O, rt, 4 h, 36%; (f) 5-benzyl-1,3,4-thiadiazol-2-amine, PyBrop, DIEA, DMF, 2 day, 20%; (g) TFA, CH_2Cl_2, 3 h, 56%.

Table 1
Modulation of R moiety: compounds **10c–y**

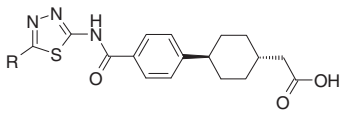

Compound	R	Enz. DGAT -1 IC_{50} (μM)	Cell. DGAT -1 IC_{50} (μM)
10		0.036	0.029
10c		0.162	ND
10d		0.085	0.588
10e		4.77	ND
10f		0.97	ND
10g		1.19	ND
10h		>10μM	ND
10i		2.84	ND
10j		1.19	ND
10k	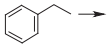	0.070	0.59
10l	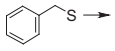	0.218	ND
10m	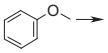	0.047	0.107
10n	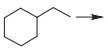	0.040	ND
10o	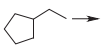	0.019	0.012
10p		0.065	0.091
10q		0.024	0.033
10r		0.426	ND
10s		0.498	ND
10t	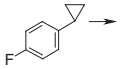	0.408	ND
10u	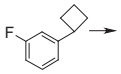	2.36	ND
10v	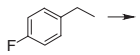	0.066	0.173
10w	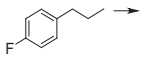	0.050	0.181
10x		0.838	ND
10y	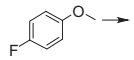	0.044	0.091

intermediate **20**. Finally, the coupling reaction followed by cleavage of the *tert*-butyl group led to the carboxylic acid **10b**.

Interestingly, with respect to modifying the amide linker, we found that the N-methyl substituted compound **21** (Fig. 6) was completely inactive.

To explore the effect of modifying the 5-substituent of the thiadiazole ring, we prepared compounds **10c–y** (Table 1). The synthetic route to derivatives **10c–y** was the same as for compound **10** (Scheme 3) using the appropriate 2-aminothiadiazole building-blocks.[16] The synthesis of the aminothiadiazole intermediate **24** is described in Scheme 5.

As shown in Table 1, while maintaining the trans-cyclohexylacetic acid moiety, we assessed different modulations at the 5-position of the thiadiazole. Introduction of a substituent at the benzylic position was tolerated (derivative **10c**) or gave less active compounds in the case of fluoro derivatives (**10t** and **10u**). The phenyl derivative **10d** retained an enzymatic IC_{50} below 100 nM, but cellular activity dropped to 588 nM. Replacing the benzyl group by a large variety of substituents (**10e–10j**) failed to give more active compounds. Finally, replacement of the phenyl moiety of **10** (benzyl) or **10k** (phenethyl) by a cyclopentyl moiety (**10q** and **10o**, respectively) gave rise to more potent inhibitors in the enzymatic test and in the cellular assay.

In order to guide further syntheses, 3D-QSAR studies were undertaken using the CoMFA[17] partial least squares (PLS) module of SYBYL 8.1.[18] Pipeline Pilot 7.5[19] was used to generate and regularize 3D molecular structures, ligand-based molecular alignment was performed[9] and Gasteiger–Hückel charges were added in SYBYL. For CoMFA analyses, we used the built-in partial least squares method in SYBYL 8.1 with pre-set parameters provided in the corresponding CoMFA module with a 2.0 Å grid spacing and a cut-off at 30 kcal/mol. A consistent model with $r^2 = 0.91$ using 3 main PLS components (estimated variance as standard error of estimate, SEE = 0.27) was derived on the representative dataset given in Table 1. The PLS analysis was repeated 10 times with five randomly selected cross-validation groups, resulting a slightly lower mean cross-validated r^2_{cv} value of 0.73. A visual representation of the steric and electrostatic fields is presented in Figure 7a which shows sterically favored (85%, green) and disfavored (15%, yellow), and anion favored 15%, red) contours on compound **10o**. Green colored areas indicate substitution points where bulky groups tend to favor protein-ligand interaction opposed to the yellow region, where steric interaction is disfavored. The red region indicates where negatively charged groups are likely to be tolerated.

Steric bulk close to the thiadiazole scaffold is unfavorable (little yellow patch, **10c**, **10f**, **10u**). However, the red patch indicates that polar linkers, particularly ethers and arylethers, are tolerated (**10m**, **10y**). Steric requirements distal to the thiadiazole scaffold are beneficial (**10i** < **10s** < **10p** < **10q** < **10o** < **10n**). The distal green patch is addressed by alkyl–aryl derivatives of the scaffold (**10**, **10k**, **10v**, **10w**), and particularly from benzyl derivatives. Although amongst the most potent inhibitors, the cycloalkyl compounds were discarded since some of them (**10n** and **10o**) suffered from high metabolic liability; they were therefore not considered for optimization (data not shown).

Since the benzyl derivative **10** was the most potent inhibitor in the enzymatic and cellular assays and displayed favorable metabolic stability, we focused our chemical efforts on the synthesis of substituted benzyl derivatives as illustrated below (Table 2). The synthetic route for preparing derivatives **25–31** was the same as for compound **10** (Scheme 3). A regression plot of the calculated versus experimentally determined log(IC_{50}) is given in Figure 7b. For the external set of compounds **25–31**, a predictive r^2 of 0.70 was obtained.

As shown in Table 2, introduction of a methoxy group in the para position led to a 20-fold loss in activity against DGAT-1 in

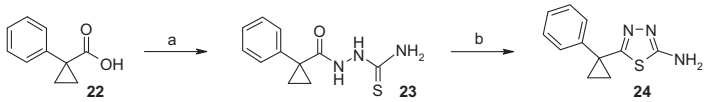

Scheme 5. Synthesis of compound **24**. Reagents and conditions: (a) thiosemicarbazide, HOBt, EDC, CH_2Cl_2 1 h, (b) H_2SO_4, rt, 8%, two steps.

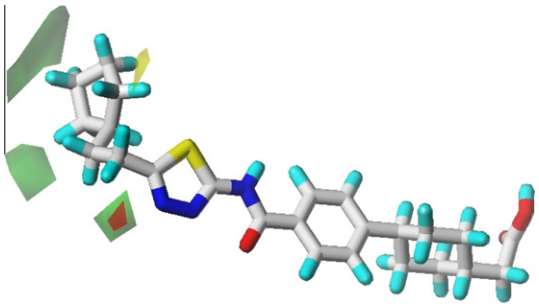

Figure 7a. Coefficient map of the CoMFA steric and electrostatic fields mapped on compound **10o**.

Table 2
Variations of the benzylic derivatives: compounds **10**, **25**–**31**

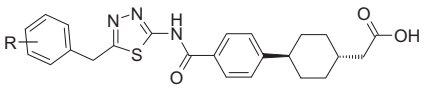

Compound	R	Enz. DGAT-1 IC_{50} (μM)	Cell. DGAT-1 IC_{50} (μM)
10	H	0.036	0.029
25	*para*-MeO	0.728	0.142
26	*para*-F	0.600	0.131
27	*meta*-F	0.030	0.046
28	*ortho*-F	0.045	0.035
29	*para*-Cl	5.28	ND
30	*meta*-Cl	0.030	0.057
31	*ortho*-Cl	0.082	ND

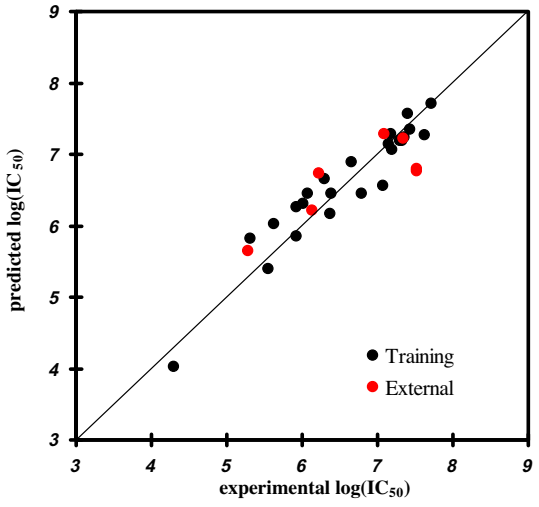

Figure 7b. Regression plot of the CoMFA predictions for the set of training compounds (Table 1) and the external prediction set (Table 2).

the enzymatic assay. The replacement of the *p*-methoxy moiety by a *p*-fluorine atom led to a slight improvement. Moving the fluorine atom to the meta or ortho position (**27** and **28**) gave rise to compounds with enzymatic and cellular activity similar to the unsubstituted compound **10**. Like the corresponding methoxy and fluorine derivatives, the *p*-chloro substitution resulted in a dramatic loss of activity. The best chloro derivative was the meta substituted compound **30**, then the ortho derivative, following the same trend as the fluoro derivatives.

Table 3
Metabolic stability and intestinal permeability

Compound	% Metabolic liability h/m[21]	Caco-2 permeability (10^{-7} cm s^{-1})[22]
10	0/5	112
27	1/10	120
28	0/4	75
30	6/14	80

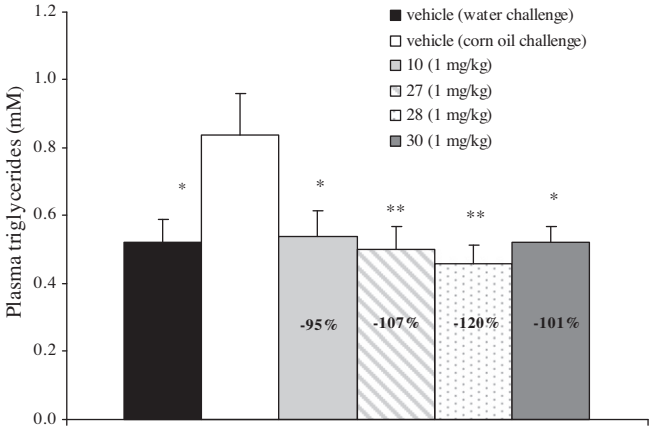

Figure 8. Lipid challenge assay.[20]

In order to assess the potential of this series in a proof-of-concept (POC) study in a pharmacological animal model, we selected the most potent benzyl derivatives (**10**, **27**, **28**, **30**) which all displayed very good metabolic stability and high intestinal permeability values (Table 3), and therefore were amenable to in vivo testing.

The pharmacodynamic effect following DGAT-1 inhibition was evaluated using an acute lipid challenge test where plasma triglycerides (TG) levels were measured after administration of an oral bolus of corn oil to fasted male C57Bl/6 J mice.[20] The administration of corn oil induced a significant rise in plasma TG levels 1 hour after the lipid bolus compared to mice treated with water (+60%; p <0.05). Tested at 1 mg/kg po 1 h before lipid challenge, compounds **10**, **27**, **28** and **30** inhibited by 95% (p <0.05), 107% (p <0.01), 120% (p <0.01) and 101% (p <0.05), respectively, the increase in plasma TG (Fig. 8). Compounds concentrations in plasma were found to be in agreement with their respective IC_{50} values, as observed for compound **10** that reached concentrations in plasma of 79.1 ± 14.8 ng/ml (181 ± 34 nM) at 1 h post-administration.

In conclusion, the combination of in silico analysis, virtual screening, parallel synthesis and ligand alignment methods has been successful in the discovery of new very potent heterocyclic DGAT-1 inhibitors. Lead optimization produced several potent inhibitors with favorable in vitro ADME properties. Advanced lead

compounds have been evaluated in a POC study in mice and shown to completely block TG production at 1 mg/kg after a lipid challenge. Further optimisation has been carried out based on these first results and will be disclosed in due course.

Acknowledgments

The authors would like to thank Jochen Görlitzer, Hans Matter, Kurt Ritter and Hans-Ludwig Schäfer for supporting the program.

References and notes

1. Reasner, C. A. *J. Cardiovasc. Pharmacol.* **2008**, *52*, 136.
2. (a) Cases, S.; Smith, S.; Zheng, Y.-W.; Myers, H. M.; Lear, R. S.; Sande, E.; Novak, S.; Collins, C.; Welch, C. B.; Lusis, A. J.; Erikson, S. K.; Farese, R. V., Jr. *Proc. Nat. Acad. Sci.* **1998**, *95*, 13018; (b) Sturley, S. L. and Oelkers, P. U.S. Pat. No. 6,100,077.
3. Cases, S.; Stone, S. J.; Zhou, P.; Yen, E.; Tow, B.; Lardizabal, K. D.; Voelker, T.; Farese, R. V., Jr. *J. Biol. Chem.* **2001**, *276*, 38870.
4. Yamaguchi, K.; Yang, L.; McCall, S.; Huang, J.; Yu, X. X.; Pandey, S. K.; Bhanot, S.; Monia, B. P.; Li, Y.-X.; Diehl, A. M. *Hepatology* **2008**, *47*, 625.
5. (a) Smith, S. J.; Cases, S.; Jensen, D. R.; Chen, H. C.; Sande, E.; Tow, B.; Sanan, D. A.; Raber, J.; Eckel, R. H.; Farese, R. V., Jr *Nature Genet.* **2000**, *25*, 87; (b) Chen, H. C.; Smith, S. J.; Ladha, Z.; Jensen, D. R.; Ferreira, L. D.; Pulawa, L. K.; McGuire, J. G.; Pitas, R. E.; Eckel, R. H.; Farese, R. V., Jr *J. Clin. Invest.* **2002**, *109*, 1049.
6. (a) Zhao, G.; Souers, A. J.; Voorbach, M.; Falls, H. D.; Droz, B.; Brodjian, S.; Lau, Y. Y.; Iyengar, R. R.; Gao, J.; Judd, A. S.; Wagaw, S. H.; Ravn, M. M.; Engstrom, K. M.; Lynch, J. K.; Mulhern, M. M.; Freeman, J.; Dayton, B. D.; Wang, X.; Grihalde, N.; Fry, D.; Beno, D. W. A.; Marsh, K. C.; Su, Z.; Diaz, G. J.; Collins, C. A.; Sham, H.; Reilly, R. M.; Michael, E.; Brune, M. E.; Kym, P. R. *J. Med. Chem.* **2008**, *51*, 380; (b) Dow, R. L.; Andrews, M.; Aspnes, G. E.; Balan, Gayatri; Gibbs, E. M.; Guzman-Perez, A.; Karki, K.; LaPerle, J. L.; Li, J.-C.; Litchfield, J.; Munchhof, M. J.; Perreault, C.; Patel, L. *Bioorg. Med. Chem. Lett.* **2011**, *21*, 6122; (c) Qian, Y.; Wertheimer, S. J.; Ahmad, M.; Cheung, A. W.-H.; Firooznia, F.; Hamilton, M. M.; Hayden, S.; Li, S.; Marcopulos, N.; McDermott, L.; Tan, J.; Yun, W.; Guo, L.; Pamidimukkala, A.; Chen, Y.; Huang, K.-S.; Ramsey, G. B.; Whittard, T.; Conde-Knape, K.; Taub, R.; Cristina, M.; Rondinone, C. M.; Tilley, J.; David Bolin, D. *J. Med. Chem.* **2011**, *54*, 2433.
7. (a) Smith, R.; Campbell, A.-M.; Coish, P.; Dai, M.; Jenkins, S.; Lowe, D.; O'Connor, S.; Su, N.; Wang, G.; Zhang, M.; Zhu, L. US2004/0224997.; (b) Fox, B. M.; Furukawa, N.; Hao, X.; Iio, K.; Inaba, T.; Jackson, S. M.; Kayser, F.; Labelle, M.; Li, K.; Matsui, T.; Mcminn, D. L.; Ogawa, N.; Rubenstein, S. M.; Sagawa, S.; Sugimoto, K.; Suzuki, M.; Tanaka, M.; Ye, G.; Yoshida, A.; Zhang, J. WO2004/047755.
8. (a) Birch, A. M.; Buckett, L. K.; Turnbull, A. V. *Curr. Opin. Drug Disc. Dev.* **2010**, *13*, 489; (b) Dow, R. L.; Li, J.-C.; Pence, M. P.; Gibbs, E. M.; LaPerle, J. L.; Litchfield, J.; Piotrowski, D. W.; Munchhof, M. J.; Manion, T. B.; Zavadoski, W. J.; Walker, G. S.; McPherson, R. K.; Tapley, S.; Sugarman, E.; Guzman-Perez, A.; DaSilva-Jardine, P. *Med. Chem. Lett.* **2011**, *2*, 407; (c) Dow, R. L.; Andrews, M.; Aspnes, G. E.; Balan, G.; Gibbs, E. M.; Guzman-Perez, A.; Karki, K.; LaPerle, J. L.; Li, J.-C.; Litchfield, J.; Munchhof, M. J.; Perreault, C.; Patel, L. *Bioorg. Med. Chem. Lett.* **2011**, *21*, 6122; (d) Citeline TrialTrove database.
9. For generating a high-quality 3D alignment we employed our internal application MARS, which performs a combinatorial analysis of ROCS 3D shape-based alignments. The program ROCS (3.1.1. (a product of OpenEye Scientific Software Inc., Santa Fe, New Mexico)) was used, which performs shape-based overlays of conformers for target molecules to the query molecule in one or multiple conformations. The ROCS algorithm maximizes the rigid overlay of atom-centered Gaussian functions and thereby maximizes the overlap between a query molecule and a single conformation of a target molecule. The MARS procedure starts from a given conformer and systematically scores each conformer of new compounds by aligning them to the optimally matched conformer. The quality of the alignment is measured on the basis of ROCS ComboScores, taking both shape and atomic features into account. This results into a matrix of similarity scores between each conformer to the others. The scores matrix is analysed to optimize alignment sets to result in a superposition with one conformer per compound. The best ranked alignment—as determined by the maximum sum of Scores—is being reported. Electrostatic maps were generated with VIDA 2.0 (a product of OpenEye Scientific Software Inc., Santa Fe, New Mexico).
10. Compound activity (0.000038 to 10 μM, final concentration) was measured in a phase-partition based assay using a recombinant human DGAT-1 enzyme (Kristie, Analytical Biochemistry, 2006, 358). Briefly, the assay was performed in 96-well Isoplate, in a 50 μl final volume, with 100 mM Hepes, 250 mM sucrose, 150 μM 1,2-di-(cis-9-octadecenoyl)-sn-glycerol, 40 μM 3*H*-octanoyl-CoA (1 μCi/ml), 10 mM $MgCl_2$ and 0.25 μg of microsomal proteins from Sf9 insect cells overexpressing human DGAT1. The reaction was initiated by the addition of DGAT1 microsomes and carried out for 60 min at 25 °C, then stopped with 10 μl of acetic acid (3.3% final concentration). After 45 min of further incubation at room temperature, 60 μl of BetaPlate Scint cocktail (Perkin–Elmer) were added in order to partition lipids from the aqueous phase. Radioactivity of the upper organic phase was determined using a MicroBeta counter (Perkin–Elmer). As confirmation of the screening, IC50s were assessed through dose–response in monoplicate. Each run was validated with a reference compound JT-553 described in the litterature[7b,8c] (IC_{50} − 28.15 nM ± 3.1, n = 207).
11. Smith, R.; O'Connor, S.; Coish, P.; Lowe, D.; Clark, R.; Stebbins, J.; Campbell, A.-M.; Akuche, C.; Shelekhin, T. WO2006/044775.
12. Compound activity was measured in vitro using Chang liver cells. Briefly, the day before the assay, cells were seeded in 24-well plates at 1.8 10^5 cells per well. The cells were starved overnight in a DMEM 4.5 g/L glucose medium supplemented with 2% Oleic Acid–Albumin complex. Thereafter, compounds were dispensed into respective wells and the plates were incubated 30 min at 37 °C, 5% CO_2. Then, the substrate (Glycerol [^{14}C] 0.4 μCi/ml final) was added into each wells and the plates were incubated 6 h at 37 °C, 5% CO_2. Incubation medium was removed and the cells were washed twice with PBS. After trypsination, cells were centrifuged for 5 minutes at 1300*g* and the supernatant was discarded. Lipids were extracted from cell pellets by adding 400 μl of a methanol/dichloromethane/TFA (50:50:0.1%) solution. The samples were sonicated and filtered (0.45 μm). The samples were analysed by HPLC (Waters 2695 with a SunFire® column C18 3 μm 4.6 × 75 mm), with a mobile phase 5% (H_2O + 0,1%TFA), 70% methanol, 25% dichloromethane with a flow of 1,5 ml/min, coupled to a flow scintillation analyzer (Perkin–Elmer radiomatic 625T) to separate and quantify the relative amount of all ^{14}C-acylglycerides formed.
13. Program ACD9 was used (a product of ACD/Labs).
14. Separation on Chiralcel OJ-H 250∗21 mm (5 μm) with a mobile phase CO_2 (MeOH + 0.5% d'isopropylamine).
15. Bovy, P. R.; Cecchi, R.; Croci, T.; Venier, O. WO2003/099772.
16. (a) Aminothiadiazole used in the synthesis are commercially available.; (b) Fett, E.; Mougenot, P.; Namane, C.; Nicolaï E. and Philippo, C. WO2010/086551.
17. (a) Cramer, R. D.; Patterson, D. E.; Bunce, J. E. *J. Am. Chem. Soc.* **1988**, *110*, 5959; (b) Clark, M.; Cramer, R. D.; Jones, D. M.; Patterson, D. E.; Simeroth, P. E. *Tetrahedron Comp. Meth.* **1990**, *3*, 47.
18. SYBYL, Tripos International, 1699 South Hanley Rd., St. Louis, Missouri, 63144, USA.
19. Pipeline Pilot 7.5, Accelrys, 10188 Telesis Court, San Diego CA 92121.
20. Lipid challenge assay: On the day of the experiment, mice were orally treated (10 mL/kg) with vehicle (0.5% methylcellulose/DMSO 1%), compounds 10, 27, 28 and 30 at 1 mg/kg (n = 10 mice per group) 1 h prior to the lipid challenge. At T0, mice were treated with 100 μL of corn oil or water. One hour after the lipid challenge (or 2 h after the treatment), blood collection was performed (intracardiac puncture) under isoflurane anesthesia. Measurement of plasma triglycerides was performed using the triglyceride determination kit from Sigma–Aldrich One way ANOVA followed by a Dunnett test was used to establish statistical significance between vehicle and treated mice. A p value below 0.05 was considered as significant ($^{*}p$ <0.05; $^{**}p$ <0.01 versus water-treated vehicle group). All the protocols used in this study were validated by the local SANOFI ethical committee.
21. Compound is incubated 20 min with human or mouse hepatic microsomal fraction. Liability % result corresponds to disappearance of tested compound at the end of the experiment.
22. (a) Grès, M.-C.; Julian, B.; Bourrié, M.; Meunier, V.; Roques, C.; Berger, M.; Boulenc, X.; Berger, Y.; Fabre, G. *Pharm. Res.* **1998**, *15*, 726; (b) Grandi, D. D.; Press, B. *Curr. Drug Metab.* **2008**, *9*, 893.